Dynamic Analysis of a Hyperbolic Composite Coupling

H. Ghoneim [a], D. J. Lawrie [b]
[a] Rochester Institute of Technology, 76 Lomb Memorial Dr. Rochester, NY 14623
[b] Lawrie Technology Inc., 227 Hathaway Street, Girard, PA 16417

ABSTRACT

A Hyperbolic novel composite coupling is proposed. In addition to enjoying the advantages of composite materials, the proposed coupling can be readily integrated with a composite drive shaft into a single unit. A mathematical model of the coupling is developed based on the Timoshenko beam theory using the energy approach and the extended Lagrange's equations. The corresponding discrete equation of vibration is obtained using the finite element method and solved for the natural frequencies using MATLAB. The dynamic characteristics of the coupling (Axial, torsional and bending natural frequencies) are studied in order to assess the merits and potential of the proposed coupling.

Keywords: Rotary dynamics, finite elements, natural frequencies and mode shapes, composite coupling.

1. INTRODUCTION

Flexible couplings transmit torque, while accommodating certain amount of misalignment, from a prime mover to a driven unit of rotating equipment [1]. Stringent demands are placed on modern flexible couplings, including: higher torque capacity, higher operational speed (at or post resonance), accommodation of more misalignments, less weight and cost. Taking advantages of the unique properties of composite materials (high specific stiffness and strength, engineering tailoring capability, and high fatigue strength and corrosion resistance), Composite coupling have been introduced in an attempt to achieve the above-mentioned demands [2,3]. This paper proposes a novel, flexible composite coupling: Hyperbolic Composite Coupling (HCC). In addition to satisfying most of the demands imposed on modern couplings, the proposed coupling can provide some needed damping [4,5]. More over, the HCC can be readily manufactured with a composite drive shaft into a single integral-coupling-drive-shaft unit [6,7], which enjoys the attractive feature of low manufacturing and maintenance cost.

The mathematical model of the proposed coupling (HCC) is derived based on the Timoshenko beam assumptions, using the energy approach and the extended Lagrange's equations [8]. Then, the discrete standard equation of vibration ($[\mathbf{M}]\ddot{\underline{U}}+[\mathbf{K}]\underline{U}=\underline{\mathbf{0}}$) is derived using the finite element method. The effect of two geometric parameters on the dynamic characteristics; more specifically, the torsional, bending and axial natural frequencies, of the proposed coupling is studied. Based on this study, the potential of the proposed coupling is addressed.

2. MATHEMATICAL MODEL OF THE COUPLING

2.1 Constitutive equation and kinematics

The model of the flexible coupling is assumed to obey the Timoshenko beam assumption. In addition, the circular cross sectional area is allowed to axially translate, rotate, and expand/contract. That is; the cross sectional circular plane remains a circular plane, but not necessarily perpendicular to the axis of the coupling (first order shear theory). Consequently, there are seven components of displacement that define the motion of a point on the cross sectional area. Based on the inertial coordinates xyz shown in Figure 1, where the x-axis coincides with the axis of the coupling, the four components of displacements that define the flexural motion of the cross section of the coupling are: the transverse displacements, u_y and u_z, and the angular rotation about the y and z axes respectively, α and β. The other three displacements are: the axial displacement, u_x, angle of twist, ϕ, and radial displacement, u_r.

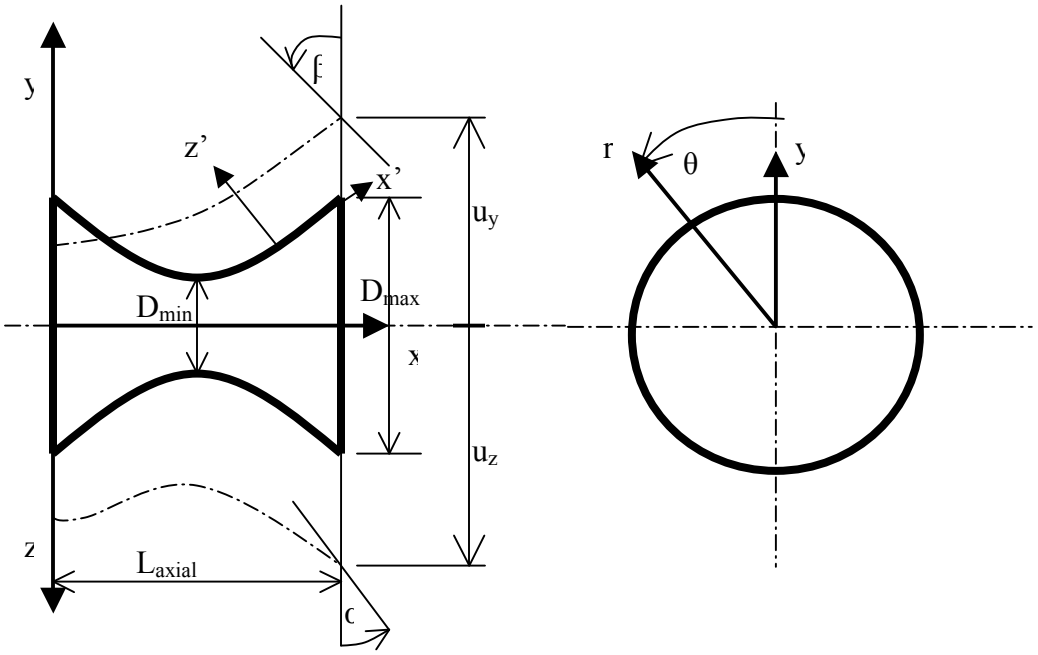

Figure 1. Schematic of the hyperboloid coupling

In the current analysis, we assume that the through-thickness stress, σ'_z, and the tangential (hoop) stress, σ_θ, are negligible. We also assume that the radial strain component, ε_r, and the inter-laminar shear strain, $\gamma_{r\theta}$, are negligible. After two sets of coordinate transformation, from material coordinates to the meridian coordinates, x'θz' (see Figure 1), and then to the global inertial cylindrical coordinates [9] xθr, the constitutive equation for any ply in the laminate of the coupling becomes,

$$\begin{pmatrix} \sigma_x \\ \sigma_r \\ \tau_{r\theta} \\ \tau_{rx} \\ \tau_{x\theta} \end{pmatrix} = \begin{bmatrix} \widetilde{Q}_{11} & \widetilde{Q}_{15} & \widetilde{Q}_{16} \\ \widetilde{Q}_{31} & \widetilde{Q}_{35} & \widetilde{Q}_{36} \\ \widetilde{Q}_{41} & \widetilde{Q}_{45} & \widetilde{Q}_{46} \\ \widetilde{Q}_{51} & \widetilde{Q}_{55} & \widetilde{Q}_{56} \\ \widetilde{Q}_{61} & \widetilde{Q}_{65} & \widetilde{Q}_{66} \end{bmatrix} \begin{pmatrix} \varepsilon_x \\ \gamma_{rx} \\ \gamma_{x\theta} \end{pmatrix} \tag{1}$$

The strain components in (1) are given by,

$$\begin{aligned} \varepsilon_x &= u'_x - (\beta' r + \beta r')\cos(\theta) + (\alpha' r + \alpha r')\sin(\theta) \\ \gamma_{x\theta} &= r\phi' + (u'_z + \alpha)\cos(\theta) - (u'_y - \beta)\sin(\theta) \\ \gamma_{rx} &= u'_r + (u'_z + \alpha)\sin(\theta) + (u'_y - \beta)\cos(\theta) \end{aligned} \tag{2}$$

The prime in equations (2) designates partial derivative with respect to x. Notice that r is a function of the axial coordinate; that is, $r = c\sqrt{\left(\left(x - L_{axial}/\mathbf{2}\right)/d\right)^{\mathbf{2}} + \mathbf{1}}$, where c and d are the two geometric parameters defining the hyperbola curve. The parameter c is the minimum radius, R_{min}, of the hyperbola.

2.2 Energy Expression

The potential energy of the coupling, U, using the assumptions introduced in equation (1), and where n is the number of layers (plies), is

$$U = \frac{1}{2}\int_0^L \sum_1^n \int_0^{2\pi} \int_{ri}^{r0} (\sigma_x \varepsilon_x + \tau_{rx}\gamma_{rx} + \tau_{x\theta}\gamma_{x\theta}) r dr d\theta dx$$

Substituting from equations (1) and (2), and after some manipulation, the expression of the coupling's potential energy becomes:

$$\begin{aligned} U = \frac{1}{2}\int_0^L \Big\{ & K_{MM}\left(\alpha'^2 + \beta'^2\right) + 2\overline{K}_{MM}\left(\beta\beta' + \alpha\alpha'\right) + \widetilde{K}_{MM}\left(\beta^2 + \alpha^2\right) \\ & + K_{VV}\left((u'_z + \alpha)^2 + (u'_y - \beta)^2\right) + 2K_{VB}\left(\alpha'(u'_z + \alpha) - \beta'(u'_y - \beta)\right) \\ & + 2K_{RB}\left(\alpha(u'_z + \alpha) - \beta(u'_y - \beta)\right) - 2K_{VA}\left(\beta'(u'_z + \alpha) + \alpha'(u'_y - \beta)\right) - 2K_{RA}\left(\beta u'_z + \alpha u'_y\right) \\ & + K_{PP}u'^2_x + K_{TT}\phi'^2 + K_{RR}u'^2_r + 2K_{PT}u'_x\phi' + 2K_{RT}u'_r\phi' + 2K_{PR}u'_x u'_r \Big\} dx \end{aligned} \tag{3}$$

The kinetic energy of the coupling is

$$T = \frac{1}{2}\int_0^L \sum_1^n \int_0^{2\pi} \int_{ri}^{ro} \rho(v_x^2 + v_y^2 + v_z^2) r dr d\theta dx$$

Upon including the gyroscopic effects, assuming small displacements and neglecting nonlinear terms, we can show that the x, y and z components of the velocities of a generic point on the shaft are, respectively:

$$\begin{aligned} v_x &= \frac{\partial}{\partial t}\{u_x - r\cos\theta\sin\beta + r\sin\theta\sin\alpha\}, \\ v_y &= \frac{\partial}{\partial t}\{u_y + r\cos\theta\cos\beta\}, \\ v_z &= \frac{\partial}{\partial t}\{u_z + r\sin\theta\cos\alpha\}. \end{aligned} \tag{4}$$

Substituting from equation (4) into the kinetic energy expression, and after some manipulation, we get

$$T_s = \frac{1}{2}\int_0^L \left\{ m(\dot{u}_x^2 + \dot{u}_y^2 + \dot{u}_z^2 + \dot{u}_r^2) + I\left(2\dot{\phi}_s^2 + \dot{\alpha}_s + \dot{\beta}_s\right) + 2I\dot{\theta}\left(\dot{\alpha}\sin\beta\cos\alpha - \dot{\beta}\sin\alpha\cos\beta\right) \right\} dx, \tag{5}$$

where, $\dot{\theta} = \Omega + \dot{\phi}$, with Ω as the spinning speed of the shaft, and is assumed constant. The dot over the letter signifies differentiation with respect to time, t. The expressions for the different stiffness, K, mass, m, and mass moment of inertia, I, in the potential energy and kinetic energy expressions can be found in the Appendix.

2.3 Mathematical model

The partial differential equation governing the dynamics of the HCC is derived using the extended Lagrange's equation [8]:

$$\frac{\partial \hat{L}}{\partial q_i}-\frac{\partial}{\partial x}\left(\frac{\partial \hat{L}}{\partial q_i'}\right)-\frac{\partial}{\partial t}\left(\frac{\partial \hat{L}}{\partial \dot{q}_i}\right)=0, \qquad 0<x<L,$$

subject to the boundary conditions: $q_i = 0$, or $\frac{\partial \hat{L}}{\partial q_i'} = 0$ at both ends (x = 0, and x = L).

In the Lagrange's equation and accompanied boundary conditions, $\hat{L} = \hat{T} - \hat{U}$, where $\hat{L}$ is the Lagrangian density, $\hat{T}$ and $\hat{U}$ are the kinetic energy density and the potential energy density, respectively. The generic displacement q_i stands for the seven displacements components, which completely define the motion of a point on the coupling. These displacements are u_x, u_r, ϕ, u_y, u_z, β and α. Substituting from (3) and (5) into the Lagrange's equation, for each displacement component, and after some manipulation, we obtain

$$\begin{aligned}
&\left(K_{PP}u_x'\right)'+\left(K_{PR}u_r'\right)'+\left(K_{PT}\phi'\right)'=m\ddot{u}_x,\\
&\left(K_{PR}u_x'\right)'+\left(K_{RR}u_r'\right)'+\left(K_{RT}\phi'\right)'=m\ddot{u}_r,\\
&\left(K_{PT}u_x'\right)'+\left(K_{RT}u_r'\right)'+\left(K_{TT}\phi'\right)'=\bar{I}\ddot{\phi}+\bar{I}\left(\ddot{\alpha}\beta-\beta\ddot{\alpha}+\alpha\beta\left(\dot{\beta}^2-\dot{\alpha}^2\right)\right)
\end{aligned} \tag{6}$$

$$\begin{aligned}
&\left\{K_{VV}\left(u_y'-\beta\right)-K_{VB}\beta'-K_{RB}\beta-K_{VA}\alpha'-K_{RA}\alpha\right\}'=m\ddot{u}_y,\\
&\left\{K_{VV}\left(u_z'+\alpha\right)+K_{VB}\alpha'+K_{RB}\alpha-K_{VA}\beta'-K_{RA}\beta\right\}'=m\ddot{u}_z,\\
&\left\{K_{MM}\beta'+\overline{K}_{MM}\beta-K_{VB}\left(u_y'-\beta\right)-K_{VA}\left(u_z'+\alpha\right)\right\}'-\overline{K}_{MM}\beta'-\widetilde{K}_{MM}\beta\\
&\quad -K_{VB}\beta'-K_{RB}\left(u_y'-2\beta\right)-K_{VA}\alpha'+K_{RA}u_z'+K_{VV}\left(u_y'-\beta\right)=I\left(\ddot{\beta}-2\Omega\dot{\alpha}-2\dot{\phi}\dot{\alpha}-\ddot{\phi}\alpha\right),\\
&\left\{K_{MM}\alpha'+\overline{K}_{MM}\alpha+K_{VB}\left(u_z'+\alpha\right)-K_{VA}\left(u_y'-\beta\right)\right\}'-\overline{K}_{MM}\alpha'-\widetilde{K}_{MM}\alpha\\
&\quad -K_{VB}\alpha'-K_{RB}\left(u_z'+2\alpha\right)+K_{VA}\beta'+K_{RA}u_y'-K_{VV}\left(u_z'+\alpha\right)=I\left(\ddot{\alpha}+2\Omega\dot{\beta}+2\dot{\phi}\dot{\beta}+\ddot{\phi}\beta\right)
\end{aligned} \tag{7}$$

Equations (6) and (7) are coupled partial differential equations that represent the axial, radial, torsional and flexural vibration of the proposed coupling. The axial, radial and torsional equations (6) are completely coupled. The transverse and rotational motions, of the flexural vibration of the coupling, are also completely coupled. Both the axial-radial-torsional vibration (6) and the flexural vibration (7) are coupled through nonlinear inertial terms. In the current analysis, these nonlinear inertial terms are ignored, which uncouples the axial-radial-torsional vibration and the flexural vibration. The appropriate boundary conditions associated with the seven equations of motions (6) and (7), respectively, are:

$$\begin{aligned}
&u_x=0, \text{ or } \left(K_{PP}u_x'\right)+\left(K_{PR}u_r'\right)+\left(K_{PT}\phi'\right)=0,\\
&u_r=0, \text{ or } \left(K_{PR}u_x'\right)+\left(K_{RR}u_r'\right)+\left(K_{RT}\phi'\right)=0,\\
&\phi=0, \text{ or } \left(K_{PT}u_x'\right)+\left(K_{RT}u_r'\right)+\left(K_{TT}\phi'\right)=0,\\
&u_y=0, \text{ or } \left\{K_{VV}\left(u_y'-\beta\right)-K_{VB}\beta'-K_{RB}\beta x-K_{VA}\alpha'-K_{RA}\alpha x\right\}=0,\\
&u_z=0, \text{ or } \left\{K_{VV}\left(u_z'+\alpha\right)+K_{VB}\alpha'+K_{RB}\alpha x-K_{VA}\beta'-K_{RA}\beta x\right\}=0,\\
&\beta=0, \text{ or } \left\{K_{MM}\beta'+\overline{K}_{MM}\beta-K_{VB}\left(u_y'-\beta\right)-K_{VA}\left(u_z'+\alpha\right)\right\}=0,\\
&\alpha=0, \text{ or } \left\{K_{MM}\alpha'+\overline{K}_{MM}\alpha+K_{VB}\left(u_z'+\alpha\right)-K_{VA}\left(u_y'-\beta\right)\right\}=0.
\end{aligned} \tag{8}$$

The coupled equations of motion (6) and (7), subjected to the boundary conditions (8), constitute the mathematical model of the proposed coupling. These equations are to be solved for the fundamental axial, torsional, and bending natural frequencies of the coupling using the finite element and MATLAB. The solution is obtained for the special case where the nonlinear inertial terms as well as the spin, Ω, are ignored.

2.4 Discrete equation of motion

Over each element the generalized displacements are expanded in terms of shape functions and nodal displacements:

$$
\begin{aligned}
&u_x(x,t) = \sum_{nn} N_i(x) U_{x\,i}(t), \quad u_r(x,t) = \sum_{nn} N_i(x) U_{r\,i}(t), \\
&\phi(x,t) = \sum_{nn} N_i(x) \Phi_i(t), \\
&u_y(x,t) = \sum_{nn} \xi_i(x) U_{y\,i}(t), \quad u_z(x,t) = \sum_{nn} \xi_i(x) U_{z\,i}(t), \\
&\alpha(x,t) = \sum_{nn} \eta_i(x) A_i(t), \quad \beta(x,t) = \sum_{nn} \eta_i(x) B_i(t),
\end{aligned}
\tag{9}
$$

Where U_{xi}, U_{ri}, Φ_i, U_{yi}, U_{zi}, A_i, and B_i are the nodal displacements, and $N_i(x)$,$\xi_i(x)$, and $\eta_i(x)$ are the shape functions. For the current analysis the cubic Hermit shape function [10] with nn = 4 is adopted for all three shape functions. Substituting (9) into the equations of motion (6) and (7), enforcing the integral of the weighted ensuing residual over the element to vanish, integrating by part to get the weak forms, and taking into consideration the appropriate boundary conditions (8), renders the element equation, $\mathbf{M}^e\ddot{\mathbf{U}}^e + \mathbf{K}^e\mathbf{U}^e = \mathbf{b}^e$, where $\mathbf{M}^e$ and $\mathbf{K}^e$ are the element mass and stiffness matrix, respectively, and $\mathbf{b}^e$ is the boundary force vector:

$$
\mathbf{M}^e = \begin{bmatrix}
\mathbf{Mx} & \mathbf{0} & \mathbf{0} & \mathbf{0} & \mathbf{0} & \mathbf{0} & \mathbf{0} \\
\mathbf{0} & \mathbf{Mr} & \mathbf{0} & \mathbf{0} & \mathbf{0} & \mathbf{0} & \mathbf{0} \\
\mathbf{0} & \mathbf{0} & \mathbf{Mp} & \mathbf{0} & \mathbf{0} & \mathbf{0} & \mathbf{0} \\
\mathbf{0} & \mathbf{0} & \mathbf{0} & \mathbf{MM} & \mathbf{0} & \mathbf{0} & \mathbf{0} \\
\mathbf{0} & \mathbf{0} & \mathbf{0} & \mathbf{0} & \mathbf{MM} & \mathbf{0} & \mathbf{0} \\
\mathbf{0} & \mathbf{0} & \mathbf{0} & \mathbf{0} & \mathbf{0} & \mathbf{JJ} & \mathbf{0} \\
\mathbf{0} & \mathbf{0} & \mathbf{0} & \mathbf{0} & \mathbf{0} & \mathbf{0} & \mathbf{JJ}
\end{bmatrix}, \quad \text{and}
\tag{10}
$$

$$
\mathbf{K}^e = \begin{bmatrix}
\mathbf{K_{xx}} & \mathbf{K_{xr}} & \mathbf{K_{xp}} & \mathbf{0} & \mathbf{0} & \mathbf{0} & \mathbf{0} \\
\mathbf{K_{xr}} & \mathbf{K_{rr}} & \mathbf{K_{rp}} & \mathbf{0} & \mathbf{0} & \mathbf{0} & \mathbf{0} \\
\mathbf{K_{xp}} & \mathbf{K_{xr}} & \mathbf{K_{pp}} & \mathbf{0} & \mathbf{0} & \mathbf{0} & \mathbf{0} \\
\mathbf{0} & \mathbf{0} & \mathbf{0} & \mathbf{+K_{uu}} & \mathbf{0} & \mathbf{-K_{ub}} & \mathbf{-K_{ua}} \\
\mathbf{0} & \mathbf{0} & \mathbf{0} & \mathbf{0} & \mathbf{+K_{uu}} & \mathbf{-K_{ua}} & \mathbf{+K_{ub}} \\
\mathbf{0} & \mathbf{0} & \mathbf{0} & \mathbf{-K_{bu}} & \mathbf{-K_{au}} & \mathbf{+K_{bb}} & \mathbf{-K_{ba}} \\
\mathbf{0} & \mathbf{0} & \mathbf{0} & \mathbf{-K_{aua}} & \mathbf{+K_{bu}} & \mathbf{+K_{ba}} & \mathbf{+K_{bb}}
\end{bmatrix}
\tag{11}
$$

Each element of the block matrices $\mathbf{M}^e$, and $\mathbf{K}^e$ is a 4x4 matrix, and the expressions of these elements are given in the Appendix. It is important to notice that, because the radius and the fiber angle orientations vary with x, all the parameters in equations (6) as well as m and J's are functions of the axial coordinate, x. Also, notice that, because of the negligence of the nonlinear inertial terms, the axial-radial-torsional (the top-left 3x3 block matrices) and the flexural (the bottom-right 4x4 block matrices) of the stiffness matrix $[K]^e$ are uncoupled. It is understood that the discrete equation of motion is recovered upon the assembly of all element equations.

3. RESULTS AND DISCUSSION

The finite element program developed for the axial-radial-torsional and flexural vibration of the composite coupling is applied to determine the fundamental axial, torsional and bending frequencies of specific coupling made up of generic carbon/epoxy. The material properties and fixed dimensions of the coupling under investigation are given in Table 1.

Dimensions and material properties	Drive shaft (T300/5208 carbon epoxy)
Maximum ~~raduis~~radius, cm (in)	7.62 (3)
Thickness, mm (in)	0.0508 (0.02)
E_1, GPa (Msi)	132 (19.2)
E_2, GPa (Msi)	10.8 (1.56)
G_{12}, Gpa (Msi)	5.56 (0.82)
G_{23}, Gpa (Msi)	3.38 (0.49)
ν_{12}	0.24
ν_{23}	0.59
ρ, kg/m^3 (lb-sec^2/in^4)	1540 (1.44x10^{-4})

Table 1 Geometric and material properties of the composite coupling

The fundamental axial, torsional and bending natural frequencies as a function of R_{min}, for the specific case of L_{axial} = 6 inches, are displayed in Figure 2. Also, shown in the Figure are the corresponding results of ANSYS. For the ANSYS results, a mesh of 16x16 (16 circumferential element x 16 axial element) shell99 composite elements is adopted. All results are conducted for the cantilevered case; that is, the fixed-free boundary conditions.

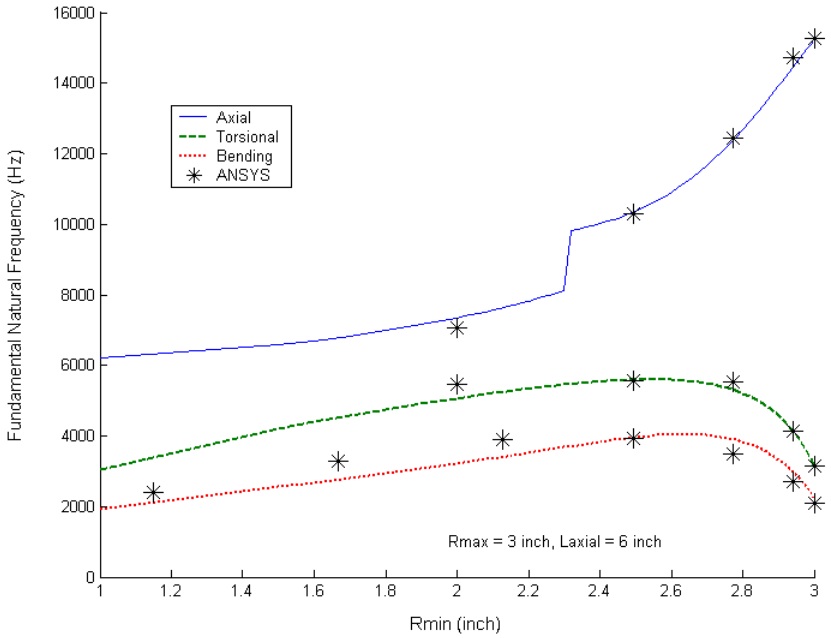

Figure 2. The variation of the fundamental natural frequencies with R_{min}

The results show a close agreement between the ANSYS and the developed finite element (FE) results. A stiffening effect of the torsional and bending modes as R_{min} is decreased from the cylindrical shape ($R_{min} = R_{max} = 3$ inches), followed by a monotonic softening effect, is depicted. The axial stiffness (natural frequency) continues to drop as R_{min} decreases. The jump phenomenon observed with the axial natural frequency will be explained later.

The effect of the coupling length (L_{axial}) and R_{min} on the fundamental torsional, bending and axial natural frequencies of the coupling is displayed, in the compound matrix of figures, in Figure 3. In general, the natural frequencies of all

three modes increase as the coupling is shortened (left-hand-side figures), and as R_{min} increases (right-hand-side figures). At small R_{min}, however, the bending natural frequency exhibits an optimum value of L_{axial} at which a

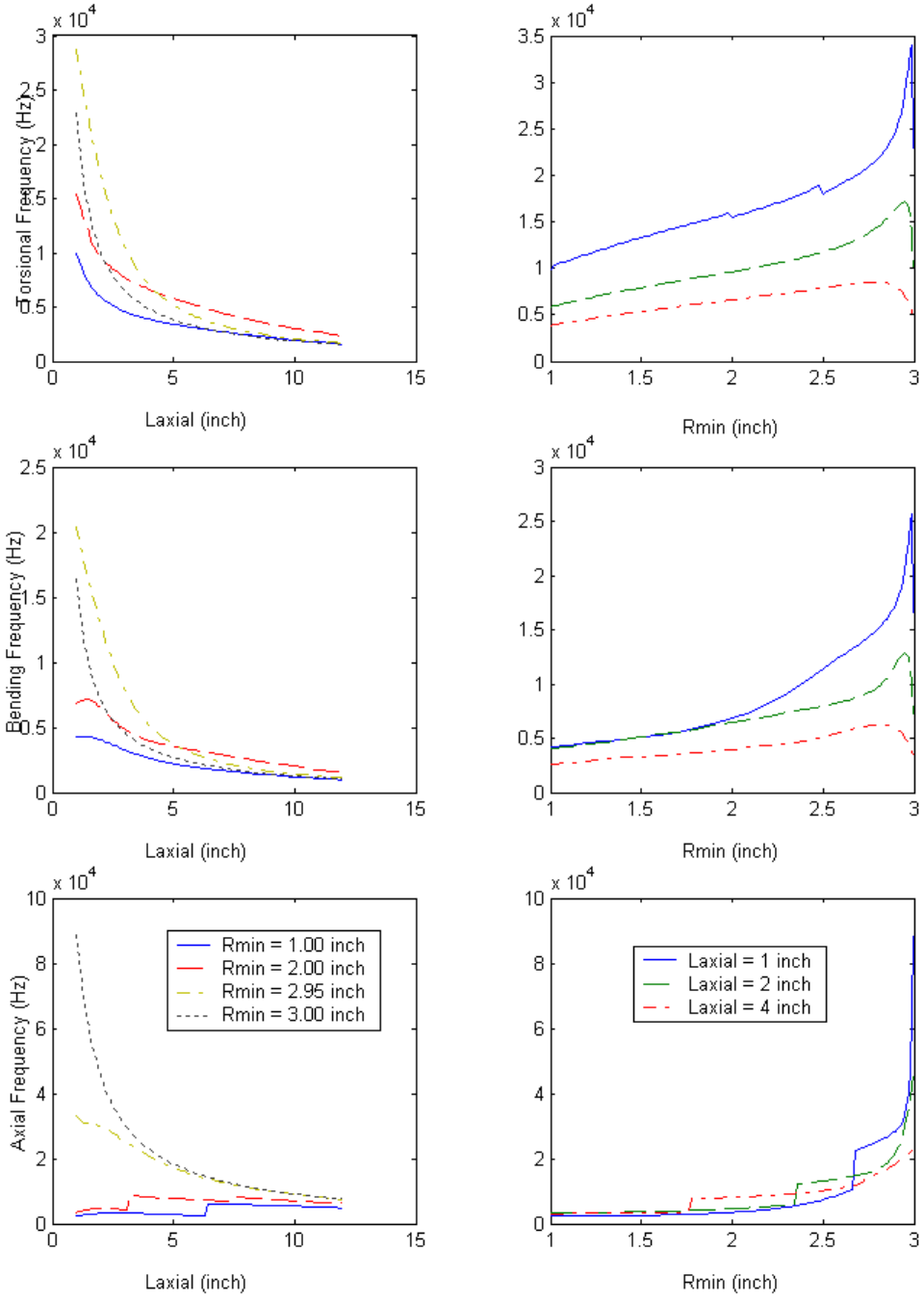

Figure 3. The effect of the L_{axial} and R_{min} on the fundamental torsional, bending and axial natural frequencies

maximum bending frequency occurs, and below which the bending frequency continues to drop as the coupling gets shorter. A peak bending as well as torsional natural frequency is also depicted as R_{min} approaches R_{max}; that is, as the hyperbolic coupling converges to a cylinder.

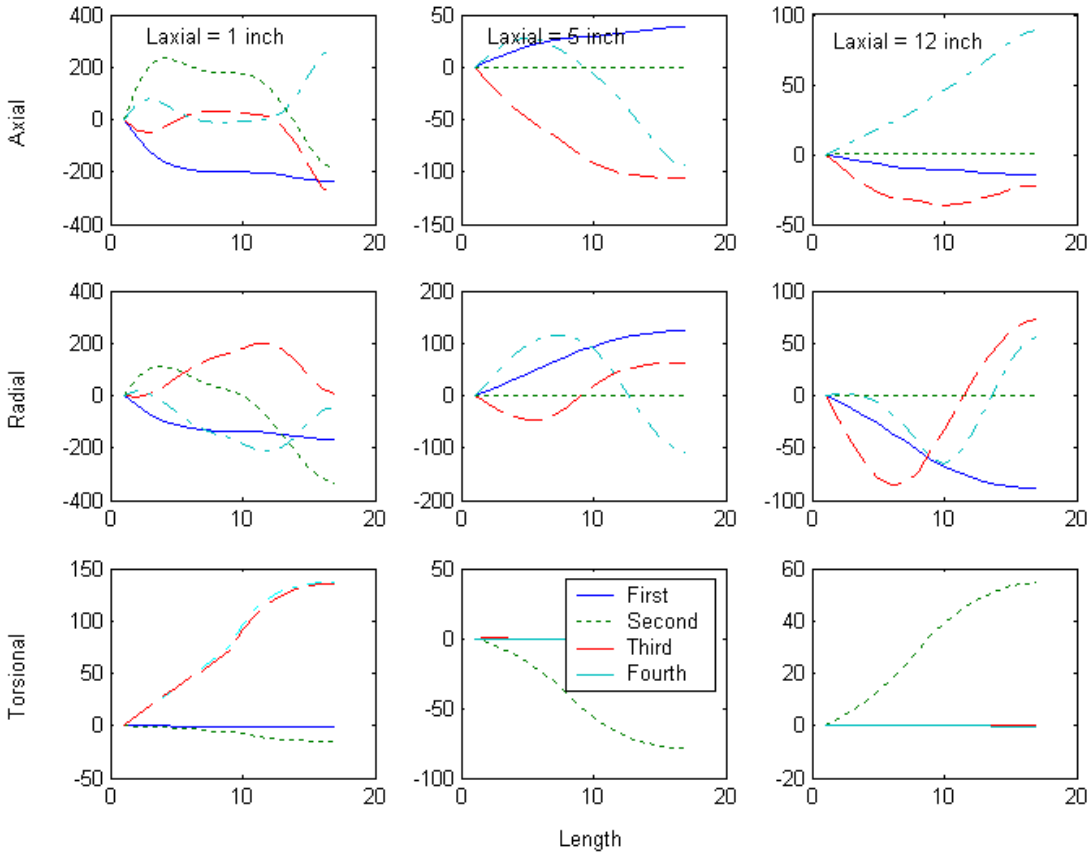

Figure 4. Axial, radial, and torsional modal displacement patterns for different coupling's axial length (R_{min} = 2 inches)

It should be mentioned that because of the full coupling among the axial, radial and torsional vibration, distinguishing among the different modes of vibration becomes a little ambiguous. In this paper, a specific mode of vibration (axial, radial, or torsional) is defined when the corresponding displacement pattern dominates the other two. For example, if all three displacements are experienced at a given natural frequency, and the axial displacement pattern dominates the other two, the mode shape is defined as the axial mode shape. This definition is responsible for the jump phenomenon exhibited in Figure 3. To explain the jump phenomenon further more, we consider the specific case of the variation of the axial natural frequency with L_{axial} for R_{min} = 2 inches (bottom-left graph in Figure 3). As L_{axial} decreases, the fundamental axial natural frequency experiences two jumps down, at $L_{axial} \approx 7.5$ and 2.5 inches. The axial, radial and torsional displacement patterns, for the lowest four natural, at L_{axial} = 1, 5, and 12 inches, are displayed in the compound matrix of figures in Figure 4. At L_{axial} = 12 inches, it is clear that the first natural frequency is the fundamental radial, the second is the fundamental torsional. However, both the third and

fourth natural frequencies demonstrate a monotonic axial displacement pattern. Since, the fourth axial displacement dominates the corresponding radial and torsional displacements, which is not the case for the third natural frequency, the fourth natural frequency is considered as the fundamental axial natural frequency. For L_{axial} = 5 inches, at the fourth natural frequency, a portion of the coupling experiences axial extension, while the other portion undergoes axial contraction. The axial displacement pattern at the third natural frequency is monotonic and dominates the corresponding radial and torsional displacement patterns. Consequently, the fundamental axial natural frequency is jumped down from the fourth to the third natural frequency. At L_{axial} = 1 inch, the axial displacement pattern is monotonic only at the first natural frequency. Also, the axial displacement dominates the other two displacement patterns (radial and torsional) and consequently, the first natural frequency becomes the fundamental axial natural frequency.

4. CONCLUSION

A novel hyperbolic coupling is presented: a hyperbolic composite coupling. In addition to enjoying the advantages of composite materials, the proposed coupling can be readily integrated with composite drive shaft into a single unit. The relevant dynamic characteristics of the coupling are investigated in this work. More specifically; the effect of two geometric parameters (minimum radius and axial length) on the axial, torsional and bending natural frequency of the coupling is studied. These three characteristics are relevant because it is recommended for an effective coupling that it ~~acquires~~acquire high torsional natural frequency (stiff in torsion) and relatively low bending and axial frequency (flexible in bending and axial deflection). A mathematical model of the coupling is developed based on the Timoshenko beam theory using the energy approach. The corresponding discrete equation of vibration is obtained using the finite element method and solved for the natural frequencies using MATLAB. The results indicate that for the proposed coupling to be viable, a short coupling with a small R_{min} is needed. Implementation of the proposed ~~coupling with a~~ composite coupling in ~~-~~to an integrated driveshaft-coupling unit, and studying the dynamic and strength characteristic of the integrated unit is the subject of future work.

5. REFERENCES

1. Anon, 2004, “Couplings and U-joints”, Motion System Dynamics: MSD A43, Vol. 12, pp 1187-1192.
2. G. Geislinger, 2003,“The geislinger gesilco advanced composite coupling with high misalignment compensation capacity and low weight,” ASME Inter Combustion Engine Division, Vol. 40, pp 65-72.
3. W. Jonathan, 2005, “Centa’s new coupling and shaft systems,” Diesel and Gas Turbine Worldwide, Vol. 37, No. 2, p 41.
4. H. Ghoneim, and D.J. Lawrie, “Analysis of flexural vibration of a composite shaft with partial cylindrical constrained layer damping treatment,” Journal of Vibration and Control, submitted for publication.
5. H. Ghoneim, and D.J. Lawrie, 2005,“Damping of a composite driveshaft,” SPIE Proceedings, Smart Structures and materials, Vol. 5760, pp 550-558.
6. H.S. Faust, E.M. Hogan, and J. Hess, 1988, “Development of an integral composite drive shaft and coupling,” American Helicopter Society: Advanced Rotorcraft Structures, Williamsburg, Virginia.
7. D.J. Lawrie, 2004, “Composite couplings/driveshaft test,” Bell Helicopter, Private Communication.
8. L. Meirovitch, 1997, “Principles and techniques of vibration,” Prentice Hall, New Jersey, pp 361-477.
9. W. Kim, A., Argento, and R. A., Scott, 1999, “Free vibration of a rotating tapered composite Timoshenko shaft,” Journal of Sound and Vibration, Vol. 226, pp. 125-147.
10. J.N. Reddy, 1993, “An Introduction to finite element method,” McGraw-Hill, New York, p. 148.

APPENDIX

The stiffness and mass expressions:

$$K_{PP} = \sum_{j=1}^{n} \pi\left(r_o^2 - r_i^2\right)_j \tilde{Q}_{11}{}^j \qquad K_{MM} = \sum_{j=1}^{n} \frac{\pi}{4}\left(r_o^4 - r_i^4\right)_j \tilde{Q}_{11}{}^j$$

$$K_{PT} = \sum_{j=1}^{n} \frac{2\pi}{3}\left(r_o^3 - r_i^3\right)_j \tilde{Q}_{16}{}^j \qquad K_{VV} = \sum_{j=1}^{n} \frac{\pi}{2}\left(r_o^2 - r_i^2\right)_j \left(\tilde{Q}_{55}{}^j + \tilde{Q}_{66}{}^j\right)$$

$$K_{PR} = \sum_{j=1}^{n} \pi\left(r_o^2 - r_i^2\right)_j \tilde{Q}_{15}{}^j \qquad K_{VA} = \sum_{j=1}^{n} \frac{\pi}{3}\left(r_o^3 - r_i^3\right)_j \tilde{Q}_{16}{}^j$$

$$K_{TT} = \sum_{j=1}^{n} \frac{\pi}{4}\left(r_o^4 - r_i^4\right)_j \tilde{Q}_{66}{}^j \qquad K_{VB} = \sum_{j=1}^{n} \frac{\pi}{3}\left(r_o^3 - r_i^3\right)_j \tilde{Q}_{15}{}^j$$

$$K_{TR} = \sum_{j=1}^{n} \frac{2\pi}{3}\left(r_o^3 - r_i^3\right)_j \tilde{Q}_{56}{}^j \qquad \overline{K}_{MM} = \left(\lambda^2 x/2\right)\sum_{j=1}^{n} \pi\left(r_o^2 - r_i^2\right)_j \tilde{Q}_{11}{}^j$$

$$K_{RR} = \sum_{j=1}^{n} \pi\left(r_o^2 - r_i^2\right)_j \tilde{Q}_{55}{}^j \qquad \tilde{K}_{MM} = \left(\lambda^4 x^2\right)\sum_{j=1}^{n} \pi \ln(r_o/r_i)_j \tilde{Q}_{11}{}^j$$

$$m = \sum_{j=1}^{n} \rho_j \pi\left(r_o^2 - r_i^2\right)_j \qquad K_{RA} = \left(\lambda^2 x\right)\sum_{j=1}^{n} \pi\left(r_o - r_i\right)_j \tilde{Q}_{16}{}^j$$

$$I = \sum_{j=1}^{n} \rho_j \frac{\pi}{4}\left(r_o^4 - r_i^4\right)_j, \ \bar{I} = 2I, \qquad K_{RB} = \left(\lambda^2 x\right)\sum_{j=1}^{n} \pi\left(r_o - r_i\right)_j \tilde{Q}_{15}{}^j$$

Where $\lambda = c/d$.

The block mass and stiffness matrices' components of the finite element analysis:

$$Mx_{ij} = Mr_{ij} = \int_0^h m(x) N_i N_j dx \qquad Kxr_{ij} = \int_0^h K_{PR}(x) N_i' N_j' dx,$$

$$Mp_{ij} = \int_0^h \bar{I}(x) N_i N_j dx \qquad Kxp_{ij} = \int_0^h K_{PT}(x) N_i' N_j' dx,$$

$$MM_{ij} = \int_0^h m(x) \xi_i \xi_j dx \qquad Krr_{ij} = \int_0^h K_{RR}(x) N_i' N_j' dx,$$

$$JJ_{ij} = \int_0^L I(x) \eta_i \eta_j dx \qquad Krp_{ij} = \int_0^h K_{TR}(x) N_i' N_j' dx,$$

$$Kxx_{ij} = \int_0^h K_{PP}(x) N_i' N_j' dx, \qquad Kpp_{ij} = \int_0^h K_{TT}(x) N_i' N_j' dx,$$

$$Kuu_{ij} = \int_0^h K_{VV}(x) \xi_i' \xi_j' dx,$$

$$Kub_{ij} = \int_0^h \left(\xi_i' K_{VB}(x) \eta_j' + \xi_i' K_{VV}(x) \eta_j + \xi_i' K_{RB}(x) \eta_j\right) dx,$$

$$Kua_{ij} = \int_0^h \left(\xi_i' K_{VA}(x) \eta_j' + \xi_i' K_{RA}(x) \eta_j\right) dx$$

$$Kau_{ij} = Kua_{ij}, \quad Kbu_{ij} = Kub_{ij}$$

$$Kbb_{ij} = \int_0^h \left(\eta_i' K_{MM}(x) \eta_j' + \left\{\eta_i' \eta_j + \eta_j' \eta_i\right\}\left\{K_{VB}(x) + \overline{K}_{MM}(x)\right\} + \eta_i \left\{K_{VV}(x) + \tilde{K}_{MM}(x) + K_{RA}(x)\right\} \eta_j\right) dx$$

$$Kba_{ij} = \int_0^h \left\{\eta_i' \eta_j - \eta_j' \eta_i\right\} K_{VA}(x) dx$$